The Astrophysical Journal, 937:86 (17pp), 2022 October 1 https://doi.org/10.3847/1538-4357/ac88c3

Investigating the Asymmetry of Magnetic Field Profiles of "Simple" Magnetic Ejecta through an Expansion-modified Flux Rope Model

Wenyuan Yu, Nada Al-Haddad, Charles J. Farrugia, Noé Lugaz, Florian Regnault, and Antoinette Galvin
University of New Hampshire, USA; wenyuan.yu@unh.edu
Received 2022 June 13; revised 2022 August 2; accepted 2022 August 9; published 2022 September 30

Abstract

Magnetic clouds (MCs) are most often fitted with flux rope models that are static and have symmetric magnetic field profiles. However, spacecraft measurements near 1 au show that MCs usually expand when propagating away from the Sun and that their magnetic field profiles are asymmetric. Both effects are expected to be related, since expansion has been shown to result in a shift of the peak of the magnetic field toward the front of the MC. In this study, we investigate the effects of expansion on the asymmetry of the total magnetic field strength profile of MCs. We restrict our study to the simplest events, i.e., those that are crossed close to the nose of the MC. From a list of 25 such "simple" events, we compare the fitting results of a specific expanding Lundquist model with those of a classical force-free circular cross-sectional static Lundquist model. We quantify the goodness of the fits by the χ^2 of the total magnetic field and identify three types of MCs: (i) those with little expansion, which are well fitted by both models; (ii) those with moderate expansion, which are well fitted by the expanding model, but not by the static model; and (iii) those with expansion, whose asymmetry of the magnetic field cannot be explained. We find that the assumption of self-similar expansion cannot explain the measured asymmetry in the magnetic field profiles of some of these magnetic ejecta (MEs). We discuss our results in terms of our understanding of the magnetic fields of the MEs and their evolution from the Sun to Earth.

Unified Astronomy Thesaurus concepts: Interplanetary magnetic fields (824); Solar wind (1534)

1. Introduction

Magnetic clouds (MCs) have been identified as a subset of the magnetic ejecta (MEs) within interplanetary coronal mass ejections (ICMEs). They were first identified by Burlaga et al. (1981) and defined by the following signatures: (i) enhanced magnetic field strength; (ii) smooth rotations of the magnetic field components through large angles; and (iii) low proton temperature or low proton beta (Klein & Burlaga 1982). They have often been associated with twisted magnetic flux ropes (Burlaga 1988; Lepping et al. 1990). Although we note that this is only one of the magnetic typologies that have been invoked to explain the in situ measurements, it is a much-used model.

MCs have been studied in depth since the 1980s. They have large spatial dimensions of order 0.2 au at 1 au, and their frequency of occurrence peaks in the solar maximum years (e.g., Richardson & Cane 2010). In addition, Moldwin et al. (1995, 2000) discovered a class of smaller flux rope structures, which have similar magnetic field structures as the MCs, but smaller observation durations. These small transients have smaller spatial dimensions, of about 0.02 au at 1 au, and, contrary to MCs, they are usually observed during the solar minimum years (Yu et al. 2014).

As a consequence, the in situ observations provide only one-dimensional measurements of the magnetic and plasma data along the spacecraft's trajectory when crossing an MC structure, so in order to understand the global spatial structure of MCs, it is necessary to consider theoretical models to describe them (e.g., Démoulin et al. 2008). The measurements of MCs obtained from spacecraft are usually fitted with models that are static, such as Lundquist's force-free cylindrically symmetric flux rope solution (Lundquist 1950), as first suggested by Burlaga (1988), and implemented by Lepping et al. (1990), which is the most widely used model, although several other models have been developed. The Lundquist model is a linear force-free model that can usually fit the three magnetic field components very well, but not the total magnetic field; the total magnetic field magnitude calculated from the fitted components is symmetric profile that peaks in the middle, whereas the observed total magnetic field of an MC typically peaks toward the beginning of the profile, or the front of the MC.

The Uniform Twist model, often referred to as the Gold–Hoyle (GH) model (Gold & Hoyle 1960; Farrugia et al. 1999), has also been proposed for studying interplanetary flux ropes. It is a nonlinear force-free model, which is also static and cylindrically symmetric, with a constant value of the magnetic line twist. This model is also able to fit the three magnetic field components very well, but again not the total magnetic field. In some cases, the GH solution can obtain better results than the Lundquist solution, particularly when the magnetic field line twist is taken into account (Hu et al. 2015; Yu et al. 2018).

In addition to these two models, several non-force-free flux rope models have been developed, for example the circular and cylindrical cross-sectional models of Hidalgo et al. (2002), Cid et al. (2002), and Hidalgo (2003, 2005). These non-force-free models produce a similar fitting quality to the force-free models (Lundquist and GH) when fitting the magnetic field components. Comparisons of several fitting models were presented in Al-Haddad et al. (2011) and Al-Haddad et al. (2018). The comparisons showed large inconsistencies in the fitting results, without a preference for any model. The results improved when the boundaries of the MCs were fixed for all fitting techniques and the fittings were performed on an isolated group of

"simple" CMEs, for which expansion was minimal and the total magnetic field was almost symmetric. However, MCs usually expand when propagating away from the Sun (Klein & Burlaga 1982), and models that include expansion are necessary in order to provide an accurate fitting. The majority of the models that include expansion assume a self-similar expansion (Farrugia et al. 1992, 1993a; Vandas et al. 2006). Farrugia et al. (1992) extended the static Lundquist model to account for self-similar expansion (Exp-Lundquist). In this model, the velocity decrease measured inside the MC is attributed to self-similar expansion, and a formalism is used to relate the magnetic field components and the velocity measurements.

Specific case studies have raised doubts in relation to the idea that the expansion is self-similar. Wang et al. (2015) introduced a quasi-steady self-similar expansion into the cylindrical force-free flux rope model. They applied this model to 72 MCs observed by the Wind spacecraft, and found that only 21% of the MCs follow a self-similar expansion at 1 au. The average expansion rate was found to be about 0.6, which means that most of the MCs underwent an underexpansion at 1 au. Conjunctions between multiple spacecraft in radial alignment have also revealed that the expansion speed at 1 au is typically not well correlated with the decrease in magnetic field as observed between the two spacecraft (Lugaz et al. 2020a). This also indicates that the expansion is unlikely to be self-similar. Recently, Davies et al. (2021) have investigated a CME measured by the Solar Orbiter and Wind, as they were in radial alignment, and the decrease in the magnetic field between the two spacecraft was not consistent with a self-similar or cylindrical symmetric configuration.

These observations and results have led us to the current investigation, which focuses primarily on the question of knowing whether or not the shift of the magnetic field peak toward the front is exclusively (or primarily) due to expansion. We also address the issue of self-similarity in these expanding structures. To do so, we compare a model of expanding flux ropes with its static counterpart to see what improvements result from taking expansion into consideration. Specifically, we take the static force-free Lundquist model and compare it with a self-similarly expanding model proposed by Farrugia et al. (1992), which called "Exp-Lundquist." We fit several "simple" ICMEs (which we call MEs) that were observed by STEREO and Wind near 1 au in the years from 1996 to 2020, whose magnetic field profiles make them particularly suitable to be fitted with the two models. The capacities of the fitting models to reproduce the magnetic field magnitude profiles are quantified and compared. The rest of the manuscript is organized as follows. In Section 2, we give a brief description of the two models used in this work. In Section 3, we present our criteria for selecting the events, as well as the ways in which we quantify the goodness of the fitting results, and present four case studies. In Section 4, we present our general results and discuss the relation between expansion and asymmetry. In Section 5, we discuss our results and conclude.

2. MC Models

2.1. Lundquist Solution

The Lundquist linear force-free solution is the most utilized technique when studying flux rope–type structures, or even all MCs in general. This solution has a symmetric magnetic field strength, with the maximum field strength always at the center, under normal assumptions (constant alpha and a circular cross section). The observed magnetic field components are usually very well fit, but not the total magnetic field. The Lundquist solution (Lundquist 1950; Lepping et al. 1990) in cylindrical polar coordinates is

$$\begin{cases} B_r = 0 \\ B_\phi = HB_0 J_1(\alpha r) \\ B_z = B_0 J_0(\alpha r), \end{cases}$$

where J_0 and J_1 are the Bessel functions of order 0 and 1, and $H = \pm 1$ is the sign of the helicity.

In most cases, α is set to $\alpha = 2.41/R$ (where R is the MC radius). This choice of α means that, at the boundaries, $B_z = 0$. For this value, $B_{\rm total}$ is symmetric, and the strength at the center is twice as large as its value at the boundaries. However, the measured magnetic fields inside ICMEs rarely match this assumption; therefore, in this study, we do not fix $\alpha = \frac{2.41}{R}$, as in the original Lundquist solution. The parameter α is still a constant value, and is a free parameter that is fitted in the Lundquist solution. We also require that $\alpha \times R$ not exceed 2.41. This ensures that the axial magnetic field inside the flux rope does not have a direction reversal. Therefore, by using the Lundquist model on the magnetic field components, the following parameters are outputs: the orientation (latitude angle, θ, and longitude angle, ϕ), impact parameter (the minimum distance between the trajectory and the axis of the MC versus the radius), B_0 (the magnetic field magnitude on the axis), H (helicity), and α (Lepping et al. 2017).

2.2. Expanding Lundquist Solution (Exp-Lundquist)

The second model that we use in this study is the expanding Lundquist solution (Exp-Lundquist), which was proposed by Farrugia et al. (1992) and further developed in Farrugia et al. (1993a). This solution considered the MC as undergoing a self-similar radial expansion, which affects the magnetic field profile.

The Exp-Lundquist model is:

$$\begin{cases} B_r = 0 \\ B_\phi = (B_0/\tau) J_1(\alpha r/\tau) \\ B_z = (B_0/\tau^2) J_0(\alpha r/\tau), \end{cases}$$

where τ is defined as $\tau = (t + t_0)/t_0$, and t_0 is the duration of the structure that has been expanding self-similarly before it encounters the spacecraft. In this solution, α is constant and is a free parameter in the fitting of the magnetic field components (we set $\frac{\alpha R}{\tau} \leqslant 2.41$). With this reconstruction method, the MC's orientations (latitude angle, θ; longitude angle, ϕ), impact parameter (the minimum distance between the trajectory and the axis versus the radius), B_0 (the magnetic field strength on the axis), and α can be outputted from fitting the B components, while t_0 is obtained from fitting the velocity profile.

We follow the two-step procedure, as highlighted in Farrugia et al. (1993a): we first fit the velocity profile to get the t_0 value, and then input the t_0 value into the expanding Lundquist solution to fit the three magnetic field components. The bulk velocity, V, profile is defined as follows: $V = V_c + \frac{r_0 - V_c \cdot t}{t - t_0} = \frac{V_c + r_0/t_0}{1 + t/t_0}$, where V_c is the average bulk speed.

The distance S from the axis of the cloud is: $S = r_0 - V_c \cdot t \rightarrow V = r/(t + t_0)$. Therefore, the expansion velocity is defined as: $V_e = \frac{V_c T}{T + 2t_0}$.

This configuration has a field strength profile that is strongly asymmetric by virtue of the expansion, and the maximum field strength is always found toward the leading edge of the cloud. Note that this configuration is not force-free, as the poloidal (ϕ) and axial (z) components of the magnetic fields change with time, and their ratio changes as τ. Further discussions on this point can be found in Farrugia et al. (1993a) and Osherovich et al. (1993).

3. Events

3.1. Event Selection Criteria: Simple ICMEs

The events under study were selected from the published lists of MEs and ICMEs as observed by STEREO (Jian et al. 2018)[1] and by the Wind spacecraft.[2] We select events, with well-defined MC-like properties, that are crossed close to the nose. In addition, the axis of the MC is required to have low inclination. With these conditions, the axis direction would have a relatively large angle as compared to the radial direction, and the maximum distance to the axis would be a small fraction of the MC radius (the impact parameter should be small). The rationale for these criteria follows the work of Farrugia et al. (1992). For such ICMEs, the expansion should occur primarily in the radial direction, removing all unknowns associated with the expansion of the MC cross section and extent in the nonradial direction (see recent results in Al-Haddad et al. 2022, for a discussion of nonradial expansion of MCs).

In more detail, we first require all the selected ICME events to have smooth rotations of the magnetic field components (the boundaries of the ICMEs that are selected depend on this criterion), and the eigenvalue ratio (mid/min) of the minimum variance analysis (MVA) of the magnetic field components to be larger than 5. This is a relatively strict criterion, as other researchers have used values of the ratio as low as 2 (Bothmer & Schwenn 1998). This ensures that the simplest model (the one derived from the MVA) has reliable results (the larger the eigenvalue ratio, the more reliable the determination of the axis orientation from the MVA.) We note that the average (median) ratio of the eigenvalues for the events presented below is 12.8 (10.3), so most events have a ratio well above our minimum criterion.

Second, we use the two Lundquist models as described above to fit these events. To keep a potential event on our list, the following criteria should be satisfied—the event should be well fitted by the original Lundquist solution, with the following specifics: (i) the orientation angles obtained from the fitting, especially the longitude angle (ϕ), should be between [60°, 120°] or [240°, 300°]; (ii) the impact parameter ($|p|$/R) obtained from the fitting should be small; and (iii) the bulk velocity should be clearly decreasing (as seen in the gradient of V).

We go through 352 ICMEs observed by STEREO and 527 ICMEs observed by the Wind spacecraft from the lists of published events cited above. By considering the criteria described above, we arrive at 25 MEs (four from STEREO and 21 from Wind) that satisfy all the criteria under the Lundquist model. By eye, all of these "simple" MEs can be decently fitted by the two Lundquist models. We note, however, that when we consider the expanding solution, there are five "simple" MEs that did not satisfy all of the criteria under the Exp-Lundquist model (having either a high inclination or a large impact parameter value in the fitting). Nonetheless, we keep these events in our analysis, as they satisfy the criteria for the original Lundquist model.

3.2. Overview

The 25 "simple" MEs are listed in the supplementary material (Table 1). The list includes the event number, the observing spacecraft, the start time and end time of the MC, the eigenvalue ratio (mid/min), the orientations (latitude angle, θ, and longitude angle, ϕ) from the MVA, the average solar wind speed, the average proton β, the average proton density, the average B_i component (the minimum eigenvector from the MVA), the ratio of $\langle B_i \rangle$ over $B_{\rm total}$, and the asymmetry of the total magnetic field component. We use three methods to quantify this asymmetry: (i) S/A, which we define as the ratio of the time to reach the maximum B divided by half of the duration of the MC—$S/A < 1$ indicates a shift toward the leading edge of the FR; (ii) $B_{\rm ratio}$, which we define as the magnetic field magnitude at the front boundary (we choose the average value of the first 20 points) divided by the magnetic field magnitude at the rear boundary (the average value of the last 20 points)—see the discussion in Farrugia et al. (1993a); and (iii) the distortion parameter (DiP), which is the duration, T_d, where the integral of $B_{\rm total}$ reaches half the total integral over the entire MC duration. DiP is made dimensionless by dividing by the total duration (Nieves-Chinchilla et al. 2018). A DiP of 0.5 indicates a "symmetric" profile, and a DiP < 0.5 implies a shift toward the front. Overall, these three measures of asymmetry are complementary, with S/A quantifying how much the peak magnetic field strength is shifted toward the front, $B_{\rm ratio}$ measuring the overall front-to-back asymmetry, and DiP measuring the overall balance of the magnetic flux within the ejecta.

We use the normalized χ^2 values to assess the fitting quality. The normalized χ^2 of the three B components is defined as

$$\chi^2 = \frac{1}{N}\sum_{i=1}^{N} \frac{(B_{xi}^m - B_{xi}^o)^2 + (B_{yi}^m - B_{yi}^o)^2 + (B_{zi}^m - B_{zi}^o)^2}{|B_{\rm total}^o|^2}.$$

In addition, the normalized χ^2 of the total B is

$$\chi^2_{B_{\rm total}} = \frac{1}{N}\sum_{i=1}^{N} \left(\frac{B_{total}^m - B_{\rm total}^o}{|B_{\rm total}^o|} \right)^2.$$

In both definitions, N is the number of measurements; m indicates the fitted quantity; o indicates the observations; B_{xi}, B_{yi}, and B_{zi} are the three components of the magnetic field; and $B_{\rm total}^o$ and $B_{\rm total}^m$ are the related total magnetic field.

The fitting procedure is based on minimizing χ^2, but χ^2 still gives an indication of how well the model fits the three components of the magnetic field. $\chi^2_{B_{total}}$ is not minimized during the fitting procedure. As such, we assess the goodness of the fits in fitting the total magnetic field by $\chi^2_{B_{total}}$. We set $\chi^2_{B_{total}} = 0.035$ as the threshold value between a good fit and a not good enough fit. This is estimated by various team members conducting a visual classification of all 50 fits (two fits for each of the 25 events) and determining a threshold that separates what the majority of members classify as good fits

[1] stereo-ssc.nascom.nasa.gov/pub/ins_data/impact/level3/ICMEs.pdf
[2] srl.caltech.edu/ACE/ASC/DATA/level3/icmetable2.htm

Table 1
MVA Results for the 25 MEs

No.	SC	Start Time	End Time	Ratio	θ_{MVA}	ϕ_{MVA}	V_{SW}	β_p	N_p	B_i	B_i/B_{total}	*S/A*	B_{ratio}	DiP
1	STB	2010-11-20/06:34:00	2010-11-21/09:10:00	25.18	4.72	62.8	409	0.027	2.44	2.58	0.245	1.03	1.09	0.489
2	Wind	1996-07-01/18:00:00	1996-07-02/10:30:00	6.22	10.82	102.92	353	0.177	17.8	−0.916	0.082	0.894	0.95	0.504
3	Wind	1998-06-02/10:30:00	1998-06-02/15:30:00	7.71	8.01	72.91	406	0.066	7.04	−0.266	0.024	0.803	0.98	0.498
4	Wind	1998-08-20/07:30:00	1998-08-21/19:00:00	21.18	−11.73	113.33	319	0.098	8.73	−2.16	0.168	0.801	0.69	0.457
5	Wind	2000-11-06/22:15:00	2000-11-07/18:15:00	11.83	−0.76	111.58	538	0.015	4.83	3.06	0.153	1.2	0.55	0.557
6	Wind	2001-04-22/00:15:00	2001-04-22/23:30:00	24.65	46.91	95.58	360	0.061	10.5	−1.45	0.12	0.669	1.17	0.453
7	Wind	2002-10-03/01:00:00	2002-10-04/18:00:00	8.81	−28.23	79.8	440	0.121	7.35	−2.44	0.223	0.824	1.19	0.475
8	Wind	2004-07-27/02:00:00	2004-07-27/15:30:00	10.31	−20.58	108	916	0.06	5.65	0.04	0.0018	0.265	1.79	0.455
9	Wind	2005-01-16/16:10:00	2005-01-17/01:25:00	6.25	4.98	67.11	540	0.115	8.86	2.02	0.221	0.632	0.97	0.504
10	Wind	2009-09-30/06:00:00	2009-10-01/00:00:00	6.98	1.95	111	342	0.365	9.19	−0.544	0.078	0.79	0.83	0.463
11	Wind	2010-05-28/19:00:00	2010-05-29/17:00:00	14.08	60.01	54.59	355	0.051	6.52	0.672	0.05	0.896	0.92	0.494
12	Wind	2012-02-14/21:00:00	2012-02-16/04:00:00	11.67	20.83	94.7	379	0.074	5.72	1.09	0.13	1.48	1.13	0.503
13	Wind	2016-10-13/06:00:00	2016-10-14/16:00:00	12.33	−22.26	97.7	385	0.021	4.49	−0.989	0.051	0.936	1.11	0.48
14	Wind	2001-03-20/00:00:00	2001-03-22/00:00:00	11.36	−54.17	131.44	367	0.012	5.62	0.167	0.011	0.579	1.39	0.416
15	Wind	2013-07-13/05:30:00	2013-07-14/23:30:00	10.2	12.26	105.74	407	0.017	3.54	−0.158	0.013	0.407	1.16	0.435
16	STA	2012-11-14/10:42:00	2012-11-16/08:45:00	5.02	53.88	77.35	381	0.051	3.17	−0.071	0.0067	0.0094	1.9	0.387
17	STA	2013-12-02/06:00:00	2013-12-04/07:40:00	13.1	46.61	125.08	508	0.017	3.82	−3.13	0.182	0.193	4.47	0.329
18	STB	2012-07-04/17:00:00	2012-07-05/12:50:00	9.99	52.11	123.65	621	0.031	4.39	−1.63	0.086	0.092	3.15	0.39
19	Wind	1997-01-10/04:40:00	1997-01-11/02:50:00	6.48	13.9	69.73	438	0.054	19.08	−2.37	0.162	1.98	0.6	0.502
20	Wind	2000-10-03/16:50:00	2000-10-05/03:00:00	14.45	4.75	71.22	403	0.044	12.2	3.01	0.223	0.337	2.02	0.417
21	Wind	2006-09-30/08:10:00	2006-09-30/19:50:00	45.19	−27.09	126.92	395	0.097	16.6	−2.76	0.168	1.04	0.89	0.488
22	Wind	2010-01-01/22:00:00	2010-01-03/10:00:00	6.47	26.19	81.58	287	0.181	8.72	−0.188	0.028	1.93	1.11	0.486
23	Wind	2012-06-16/23:00:00	2012-06-17/12:00:00	6.13	−40.17	96.8	443	0.09	22.6	2.49	0.086	0.108	3.07	0.375
24	Wind	2012-11-01/00:00:00	2012-11-03/00:00:00	14.57	78.59	113.4	326	0.204	9.9	0.652	0.078	0.0056	5.98	0.332
25	Wind	2015-09-08/00:00:00	2015-09-09/15:00:00	9.38	1.95	82.47	460	0.101	12.4	3.3	0.244	0.445	1.5	0.379

from the not so good fits. Most or part of the asymmetry of $B_{\rm total}$ might be due to expansion. When this is the case, the Exp-Lundquist model is able to obtain a better fitting on $B_{\rm total}$, as quantified by a smaller value of $\chi^2_{B_{total}}$. We therefore compare the normalized χ^2 values of these two models. Based on this methodology and our threshold, we identify three types of MEs: (i) Type 1s—those that are well fitted by both models, i.e., where $\chi^2_{B_{total}}$ is less than 0.035 for both models (events 1–13); (ii) Type 2s—those that are well fitted by the expanding model, but not by the static model (events 14 and 15); and (iii) Type 3s—those that are not adequately fitted by either model (events 16–25). We present four typical ME examples from this study (one from the STEREO-B spacecraft and three from Wind), as detailed below. We include two examples of Type 1 events and one example of Type 2 and 3 events.

In Figures 1, 2, 3, and 4, the black lines indicate the observed data, while the ejecta intervals occur between the two vertical black dashed lines. The panels show $B_{\rm total}$ and the three B components (in RTN coordinate, when observed by the STEREO spacecraft, and in the GSE coordinate system, when observed by the Wind spacecraft). In the panels for $B_{\rm total}$ and the three B components, the red lines are fit with the Lundquist model and the green lines are fit with the Exp-Lundquist model, followed by the proton velocity (the green line in this panel is the fit to V_p, which is considered the self-similar expansion, t_0), proton density, temperature (black shows the proton temperature and red shows the expected temperature, following Lopez 1987), Alfvén mach number, and β_p, respectively.

For each event, we calculate the dimensionless expansion rate (ζ), which is defined as $\zeta = \frac{V_e}{V_c} \cdot \frac{d}{R}$, where $d \sim 1$ au is the distance from which the measurements were taken and the other symbols are as previously described. This follows the definitions of Démoulin et al. (2008) and Gulisano et al. (2010), although it is exactly identical only when the velocity is linearly decreasing throughout the event. The average value of ζ near 1 au is 0.8 for undisturbed MCs (Gulisano et al. 2010).

3.3. Case1 (Event 2): Wind-19960701

Case 1 (Event 2) is shown in Figure 1. This event was observed by Wind from 1996 July 1 18:00:00 to 1996 July 2 10:30:00, as shown in Figure 1. This event is well fitted for both models (Type 1), with $\chi^2_{B_{total}} = 0.013$ and 0.012 for the Lundquist and Exp-Lundquist models, respectively. This indicates that both models fit the data equally well. This is a slow event, with an average speed of 353 km s^{-1}, which was propagating within slow solar wind (with a pre-event speed of about 320 km s^{-1}). The average proton beta is around 0.2, indicating a magnetically dominated ejecta. The ejecta were not preceded by a shock, but were nonetheless preceded by a sheath with an enhanced magnetic field and density, and a slowly rising velocity. The ability of such slow ICMEs to drive a sheath has recently been discussed in Salman et al. (2020). The MVA returns an eigenvalue ratio of 6.2, and the orientation of this flux rope is (10.°8, 103°) in GSE coordinates, i.e., a low-lying event crossing close to the nose. This is also clear from the profiles of B_y and B_z, which show a south–west–north event, following the classification of Bothmer & Schwenn (1998), i.e., an event with the B_z component going from negative to positive, while the B_y component remains positive. Comparing the fitting results of the Lundquist and the Exp-Lundquist solutions, which have the orientations (9.°6, 88°) and (9.°9, 97°), respectively, the axes from the fittings with the different models are very close in orientation, and consistent with the MVA results. The radius of this event, from both fittings, is around 0.07 au, indicating a small event (the average value at 1 au is ∼0.1–0.12 au), and the magnetic field magnitude on the axis is around 12.5 nT, which is relatively typical. The impact parameters of the two models are 0.27 and 0.15, i.e., small in both cases, as is clear from the low, but nonzero, value of B_x.

The decrease of the proton velocity along the spacecraft path is very small, and the expansion velocity (V_e) obtained from the velocity profile is just 11.6 km s^{-1} (almost no expansion). For this event, the expansion rate is 0.47, which is small, and classified as underexpanding. For the first step of the fitting with the Exp-Lundquist model, we find a value of $t_0 = 242$ hr (about 10 days), which is very large. It is highly unlikely that the ME has been expanding self-similarly for such a long amount of time, since most slow ICMEs take about 5 days to propagate from the Sun to the Earth. The boundary value ($\alpha R = 2.16$) is from the Lundquist fitting, the αR is 2.15 from the Exp-Lundquist solution, with $\alpha R/\tau = 2$.

We next turn our attention to the measure of asymmetry. This event has a DiP of 0.50, a front-to-back magnetic field ratio of 0.95, and the peak magnetic field is slightly shifted toward the front, with $S/A = 0.89$. Overall, this confirms the visual inspection, which indicates a relatively symmetric magnetic field profile. As such, it confirms that force-free constant-alpha models, such as the Lundquist model, are well able to fit events with low expansion and low asymmetry of the magnetic field vector. For such events, however, the value of t_0 may not adequately correspond to the time for which the event has been expanding self-similarly, as is assumed.

3.4. Case2 (Event 8): Wind-20040727

Case 2 (Event 8) is shown in Figure 2. This event was observed by Wind from 2004 July 27 02:00 UT to 2004 July 27 15:30 UT. This event had strong expansion, and the quality of the fit is somewhat improved by the Exp-Lundquist solution (Type 1), with $\chi^2_{B_{total}} = 0.019$ (as compared to the Lundquist model, where $\chi^2_{B_{total}} = 0.027$).

This is a fast ME, with an average speed of around 916 km s^{-1}. The average β_p is small (0.06) and symmetric, and is at its minimum around the center. N_p is around 5.7 cm^{-3}. From the MVA, the eigenvalue ratio is 10.3. This is large, and it indicates that the results provide well-defined directions. The orientation of this ME from the MVA is (−20.°6, 108°) in GSE coordinates, which is close to that found by the Lundquist and the Exp-Lundquist models ((−27.°7, 112°) and (−26.°5, 123°), respectively). The radius of this ME is around 0.14 au, from the Lundquist model, and 0.13 au, from the Exp-Lundquist model (close to the average size of MCs at 1 au). In addition, the magnetic field component relating to the minimum eigenvalue is very small (the fraction of the average B_i to $B_{\rm total}$ is less than 0.002), which means that the impact parameter of this event is very small. This is confirmed by the impact parameters obtained from both of the fitting models: 0.033 versus 0.161.

The expansion speed of this event is 119 km s^{-1} (a large decrease in the V_p profile), which corresponds to about 13% of the ME center's speed. The expansion rate (ζ) is 0.989, which implies that the MC is undergoing a self-similar expansion process, although the value is higher than the average value of 0.8 for unperturbed MEs. Through fitting the V_p profile, we obtain $t_0 = 45.3$ hr (about 2 days). This fast "simple" ME is expected to

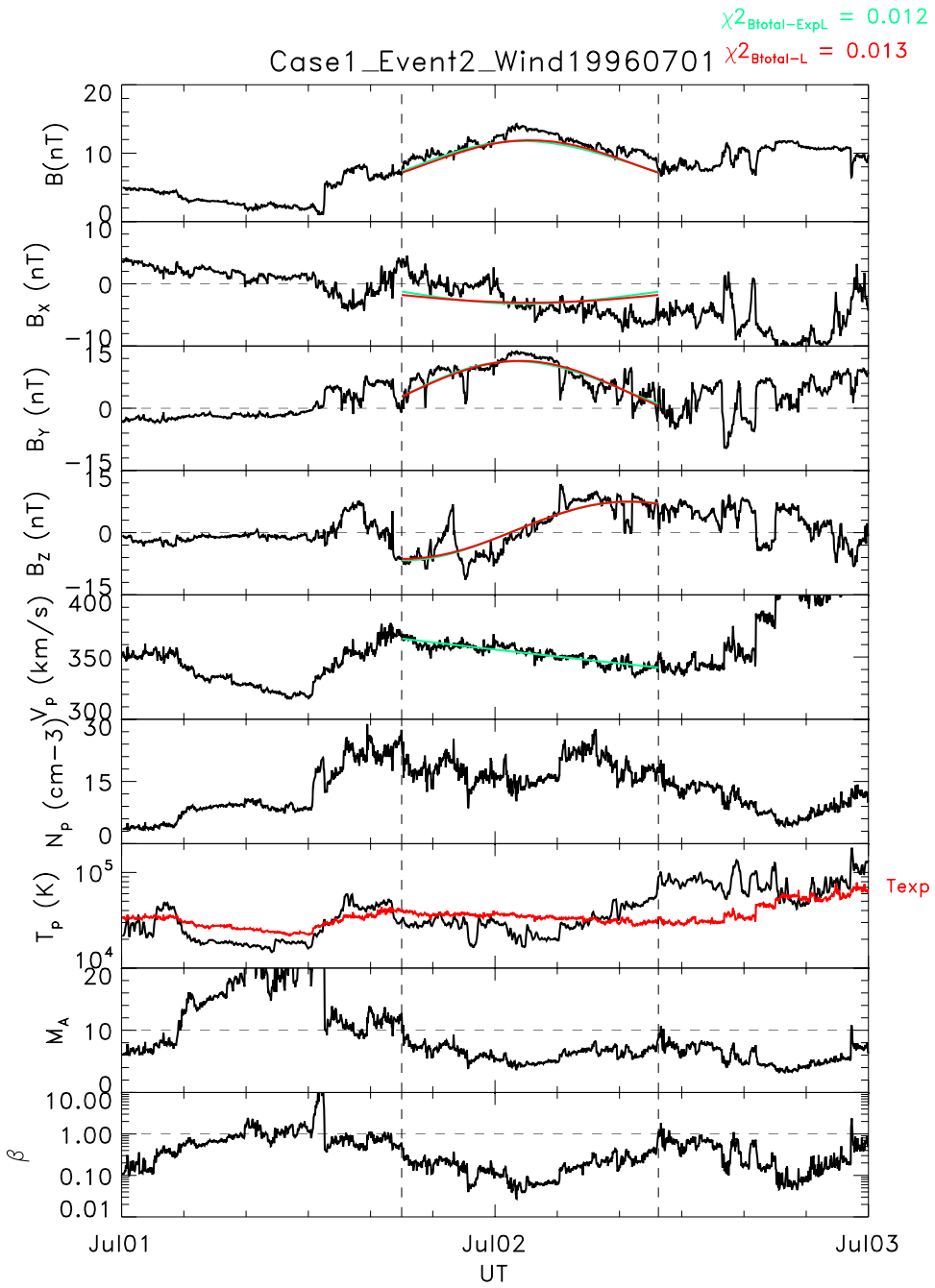

Figure 1. Wind measurements and fitting results for the ME interval (vertical black dashed lines) from 1996 July 1 18:00 UT to July 2 10:30 UT for a Type 1 event. The panels show $B_{\rm total}$, the three B components in GSE coordinates, the proton velocity, proton density, proton temperature (the red line is the expected temperature), Alfvén mach number, and β_p, from top to bottom, respectively. In the top four panels, the black lines indicate the observations, the red lines indicate the fit with the Lundquist model, and the green lines indicate the fit with the Exp-Lundquist model.

take about 2 days to propagate from the Sun to 1 au, so the value of t_0 is consistent with the propagation time, as hypothesized in Farrugia et al. (1993a). The self-similar expanding time t_0 is consistent with the propagation time.

$B_{\rm total}$ is mildly asymmetric, with a DiP value of 0.455. The peak of the magnetic field profile is close to the front boundary ($S/A = 0.265$). The field at the front boundary is stronger than at the rear boundary ($B_{ratio} = 1.79$), but the profile does not deviate significantly from that expected for a force-free structure. Both fitting models can fit the magnetic field components very well (the normalized χ^2 are 0.184 versus 0.169). The Lundquist model fits the rear half of the $B_{\rm total}$ well, but not the front half. The Exp-Lundquist model's fitting of the $B_{\rm total}$ leads to a small but noticeable improvement of the fit (the normalized χ^2 are 0.027 versus 0.019). Overall, this shows a Type 1 event (well fitted by both models) with large expansion. It shows that some events undergo self-similar expansion and can be well fitted by force-free models (with or without expansion).

3.5. Case3 (Event 14): Wind-20010320

Case 3 (event 14) is shown in Figure 3. This event was observed by Wind from 2001 March 20 00:00 UT to 2001 March 22 00:00 UT. This event had a moderate expansion

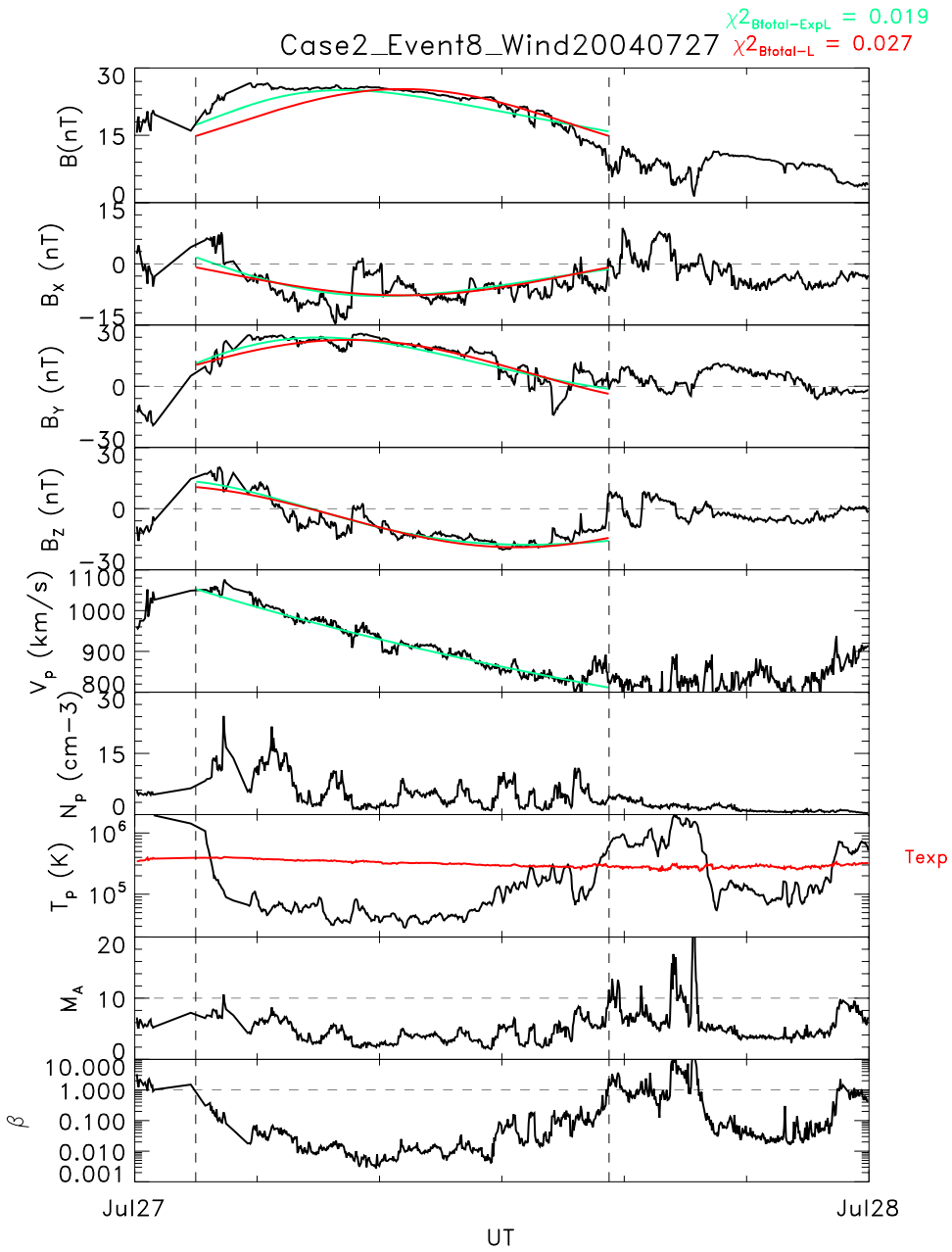

Figure 2. Wind: 2004 July 27 02:00:00–2004 July 27 15:30:00 (Type 1). The same format as Figure 1.

(73 km s^{-1}), and the fitting was significantly improved with the Exp-Lundquist solution (Type 2; $\chi^2_{B_{total}} = 0.044$ for the Lundquist model and 0.02 for the Exp-Lundquist model).

This event has a very low β_p (0.012), indicating a strongly magnetically dominated structure, which would typically be well fitted by force-free models. There is a sheath structure in front of this "simple" ME, with enhanced magnetic field, proton density, and velocity. From the MVA, the obtained eigenvalue ratio (mid/min) is 11.4, again indicating very good results. The ME axis orientations are (−54.°2, 131°), (−51.°2, 90°), and (−44.°8, 75°) in GSE coordinates for the MVA, Lundquist, and Exp-Lundquist solutions, respectively. The radius, from both models, is around 0.215 au (larger than typical MEs). The impact parameters from the two models are 0.206 and 0.248, which are consistent with the nonzero value of B_x in the front half. The boundary value ($\alpha R = 2.4$) is from the Lundquist fitting, while the αR is 3.25 from the Exp-Lundquist solution, with $\alpha R/\tau = 2.18$. The difference between the front and rear boundaries is due to the asymmetry of $B_{\rm total}$.

This ME propagates with an average speed of 367 km s^{-1}, and while the expansion speed is moderate, the ratio of the expansion to the center speeds is 20%, i.e., the ME expansion is large, as compared to its propagation speed. This represents an event for which expansion is a significant contributor to the formation of a sheath region (Lugaz et al. 2017; Salman et al. 2020). With the large expansion, as compared to propagation speed, the expansion rate (ζ) is about 0.921, which supports self-similar expansion, but is again larger than average. t_0 obtained from fitting the velocity profile is 97 hr (about 4 days). Again, based on the average ME speed of 367 km s^{-1}, this value of t_0 corresponds to the expected propagation time of

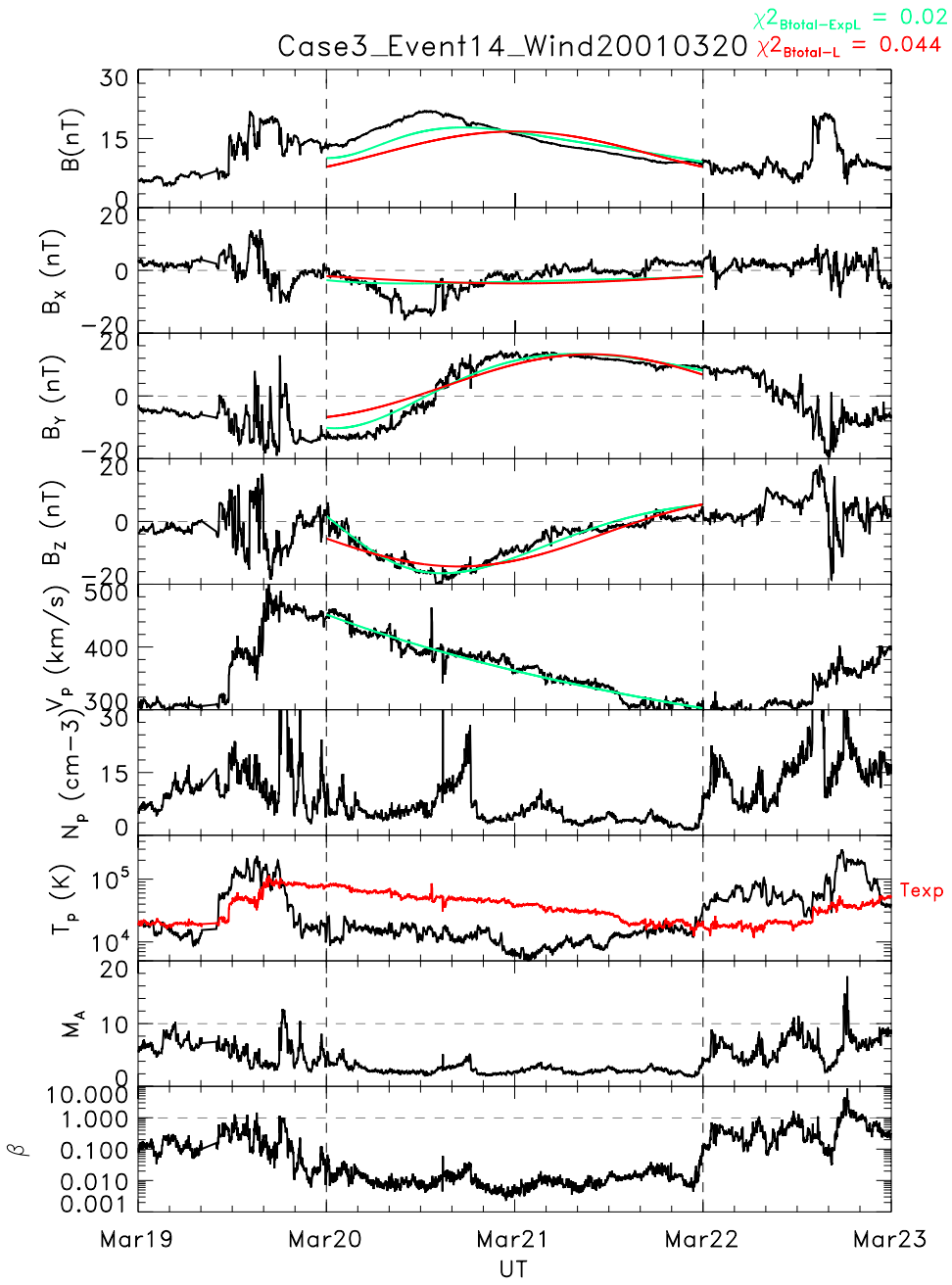

Figure 3. Wind: 2001 March 20 00:00:00–2001 March 22 00:00:00 (Type 2). The same format as Figure 1.

80–100 hr. This indicates that this ME may be propagating self-similarly from the Sun to the Earth.

$B_{\rm total}$ of this event is very asymmetric, with a DiP value of 0.416. The peak of the magnetic field profile is close to the front quarter of the ME, with $S/A = 0.58$, followed by a long tail. The field at the front boundary is slightly stronger than that at the rear boundary ($B_{ratio} = 1.39$). The fittings of the magnetic field components and $B_{\rm total}$ are all improved by using the Exp-Lundquist model (the normalized χ^2 of the magnetic field components and $B_{\rm total}$ are smaller with the Exp-Lundquist solution: 0.13 and 0.02 versus 0.204 and 0.044, respectively). Overall, this event can be well explained as a relatively slow ME that experiences a long (4.5 days) self-similar evolution, with a large expansion speed as compared to its propagation speed. The speed profile shows a clear expansion, which explains the shift of the peak of the magnetic field toward the front, the DiP being lower than 0.5, and the higher magnetic field strength at the front as compared to the back. However, $B_{\rm total}$ cannot be completely reproduced with the self-similar expanding Lundquist model. Therefore, we can conclude that the asymmetry of the total magnetic field is partly due to self-similar expansion, but also to other factors.

3.6. Case4 (Event 18): STB-20120704

Case 4 (Event 18) is shown in Figure 4. This event was observed by STEREO-B from 2012 July 4 17:00 UT to 2012 July 5 12:50 UT. This is a fast ME (an average speed of 620 km s^{-1}), with a moderate expansion (84 km s^{-1}). Both models failed to obtain good fittings on $B_{\rm total}$ (the χ^2 of $B_{\rm total}$

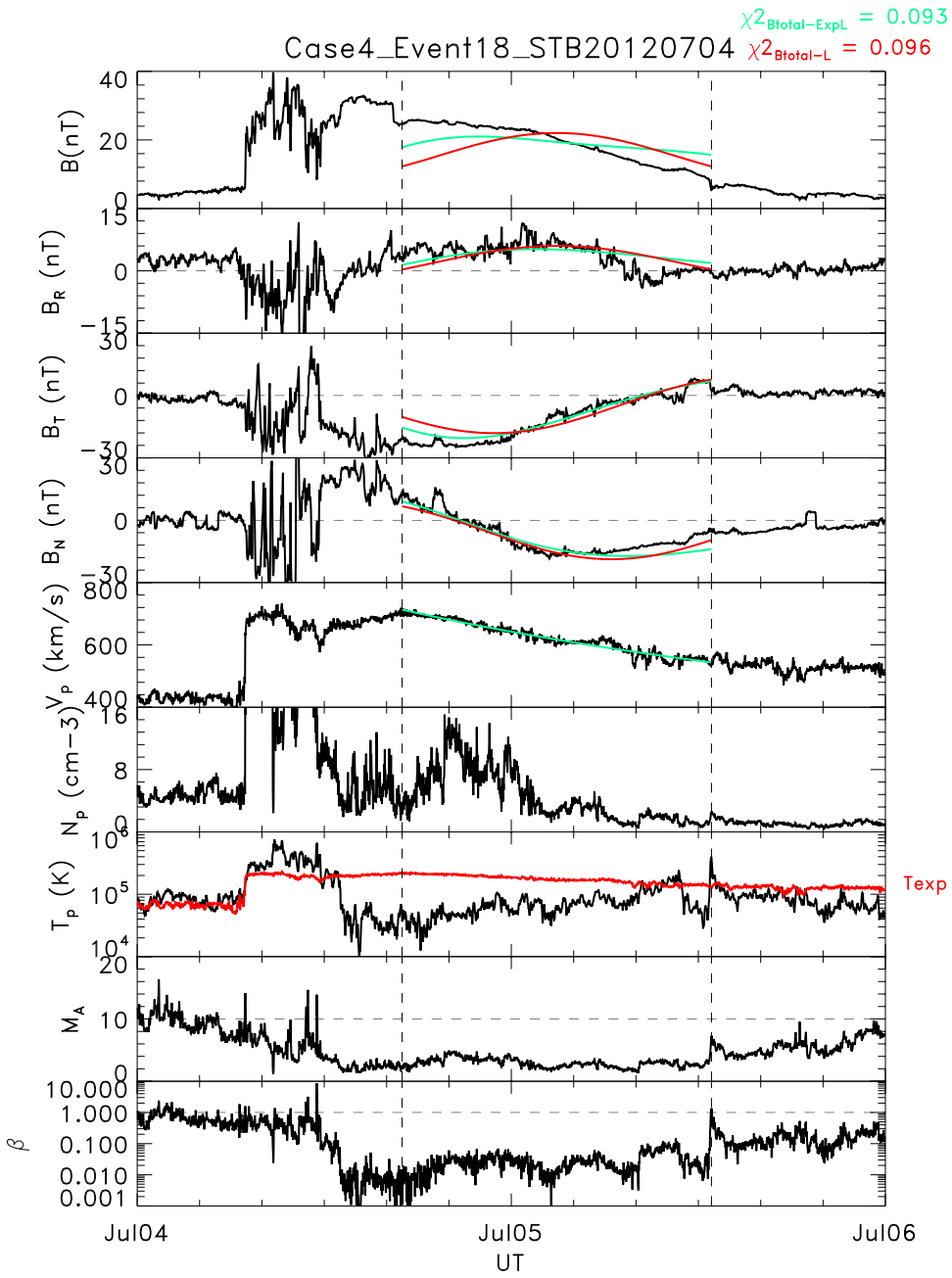

Figure 4. STEREO-B: 2012 July 4 17:00:00–2012 July 5 12:50:00 (Type 3). The same format as Figure 1, but the magnetic field data are in RTN coordinates.

are 0.096 for the Lundquist and 0.093 for the Exp-Lundquist solutions), which makes this a Type 3 event.

This ME is preceded by a sheath region and a shock. The average of β_p inside the ME is 0.031, indicating magnetically dominated ejecta. The eigenvalue ratio obtained by the MVA is around 10, and the orientation of this ME is (52°.1, 124°) in RTN coordinates. Comparing the orientations obtained from both the fitting models ((−45°.1, 295°) for the Lundquist solution and (−47°.2, 288°) for the Exp-Lundquist solution), the axes have reverse signs, but the directions of the axes are consistent overall. The values for the radius from these two models are consistent with each other (around 0.145 au). The dimensionless impact parameters from both models are small (0.023 versus 0.041), indicating a crossing that reaches very close to the axis. The boundary value ($\alpha R = 2.24$) of the Lundquist solution is between the two boundary values of Exp-Lundquist solution (2.7 and 2.06), and the difference can easily be seen in the $B_{\rm total}$ plot in Figure 4.

Both models fit the B components well and the normalized χ^2 value of the Lundquist solution is better (0.166, slightly less than the value of 0.176 from the Exp-Lundquist solution). However, neither of the solutions fit $B_{\rm total}$ well. The normalized χ^2 of $B_{\rm total}$ are large for both models (0.096 and 0.093, respectively). The expansion speed from the velocity profile is 84 km s^{-1}, corresponding to a ratio of expansion to propagation speeds of 13.5%, and the expansion rate (ζ) is 0.928, also indicating a self-similar expansion, similar to the previous examples.

$B_{\rm total}$ of this event is very asymmetric, with a DiP value of 0.39. The peak is near the front boundary, with $S/A = 0.092$, and the profile is close to monotonically decreasing through the ME. The field at the front boundary is much larger than that at

Table 2
Fitting Results of 25 MEs (Lundquist Solution)

No.	θ_L	ϕ_L	$\lvert p\rvert/R_L$	R_L	B_{0L}	H_L	αR_L	χ^2_L	$\chi^2_{B_{totalL}}$
1	21.53	86.14	0.465	0.148	13.32	+	2.4	0.161	0.015
2	9.64	88.06	0.266	0.073	12.39	⋯	2.16	0.201	0.013
3	12.5	79.33	0.061	0.024	11.91	⋯	1.56	0.042	0.0011
4	−3.14	277.73	0.083	0.135	14.25	+	2.4	0.253	0.026
5	6.09	112.76	0.149	0.121	23.02	⋯	2.05	0.092	0.022
6	−50.32	288.26	0.208	0.101	14.41	⋯	2.2	0.071	0.018
7	−30.21	81.83	0.21	0.22	12.18	+	2.4	0.208	0.03
8	−27.73	112.48	0.033	0.14	25.32	+	2.12	0.184	0.027
9	0.62	263.76	0.035	0.06	10.04	⋯	2.01	0.107	0.017
10	9.5	304.64	0.182	0.062	8.09	⋯	2.35	0.227	0.031
11	−61.73	242.06	0.014	0.091	15.33	⋯	2.36	0.116	0.023
12	−32.6	262.66	0.187	0.143	9.44	+	2.4	0.188	0.032
13	−19.42	90.01	0.124	0.159	22.99	⋯	2.41	0.099	0.007
14	−51.19	90.34	0.206	0.216	17.05	⋯	2.4	0.204	0.044
15	−27.05	277.43	0.089	0.205	14.05	⋯	2.4	0.135	0.05
16	−62.63	262.91	0.058	0.211	11.82	+	2.28	0.19	0.085
17	−79.08	113.08	0.42	0.333	18.3	⋯	2.4	0.601	0.151
18	−45.14	294.84	0.023	0.142	22.03	+	2.24	0.166	0.096
19	−15	262.12	0.311	0.122	17.56	+	2.41	0.123	0.041
20	−4.89	91.22	0.46	0.187	15.34	+	2.41	0.401	0.061
21	30.45	277.08	0.072	0.055	15.99	⋯	2.4	0.383	0.061
22	25.28	76.51	0.082	0.122	7.15	+	2.3	0.22	0.051
23	−16.58	94.25	0.085	0.069	32.31	+	2.07	0.288	0.137
24	−45.61	283.4	0.027	0.186	6.65	+	2.4	1.02	0.194
25	15.02	89.31	0.61	0.335	14.29	+	2.41	0.85	0.112

the rear boundary ($B_{ratio} = 3.15$). This strong asymmetry of $B_{\rm total}$ cannot be reconstructed well by either model. In this event, t_0 is 64 hr (about 2.5 days), and the average ME speed is 621 km s^{-1}, which results in an estimated propagation time of about 70 hr. This confirms that this ME is propagating self-similarly from the Sun to the Earth. Therefore, in this case, the asymmetry is not only due to self-similar expansion, but also to other possible factors.

4. Overall Results

4.1. Fitting Results

The fitting results of these 25 MEs are shown in the supplementary materials (Table 2 shows the Lundquist model outputs and Table 3 shows the Exp-Lundquist model outputs).

In Tables 2 and 3, we show (i) the event number; (ii) θ, the latitude angle (°) of the fitted axis in the GSE (Wind) or RTN (STEREO) coordinate systems; (iii) ϕ, the longitude angle (°) of the axis in the same coordinate systems; (iv) the dimensionless impact parameter $|p|/R$; (v) the radius obtained from fitting R in au; (vi) B_0, the magnetic field magnitude on the axis obtained from fitting in nT; (vii) H, the sign of helicity (± 1); (viii) αR, α times the radius (which provides the boundary information; $\alpha R = 2.41$ means that $B_z = 0$ at the boundary); (ix) χ^2, the reduced normalized chi-square of the B components, which is minimized during the fitting procedure; (x) and $\chi^2_{B_{total}}$, the reduced normalized χ^2 of $B_{\rm total}$. The definitions of χ^2 and $\chi^2_{B_{total}}$ are described above. In Table 3, we provide the additional following information: (ix) $\alpha R/\tau$, which provides the information at the rear boundary; (x) t_0, the time for which the cloud has been expanding, as obtained from fitting the speed profile (h); (xi) V_e, the expansion velocity (km s^{-1}); (xii) $V_e/\langle V\rangle$, the expansion velocity relative to the average speed of the ejecta; and (xiii) ζ, the dimensionless expansion rate.

4.2. Fitting Output Parameters

The scatter distributions of the output parameters of the two fitting models are presented in Figure 5: (a) latitude angle, θ (°); (b) longitude angle, ϕ (°); (c) B_0 on the axis of the model (nT); (d) fitted radius (au); (e) the αR of the Lundquist model versus

Table 3
Fitting Results of 25 MEs (Exp-Lundquist Solution)

No.	$\theta_{\rm ExpL}$	$\phi_{\rm ExpL}$	$\lvert p\rvert/R_{\rm ExpL}$	$R_{\rm ExpL}$	$B_{0\rm ExpL}$	$H_{\rm ExpL}$	$\alpha R_{\rm ExpL}$	$\alpha R/\tau_{\rm ExpL}$	$t_{0\rm ExpL}$	$V_{e\rm ExpL}$	V_e/V	ζ	$\chi^2_{\rm ExpL}$	$\chi^2_{B_{\rm totalExpL}}$
1	24.6	89.18	0.39	0.142	18.69	+	3.17	2.41	83.87	55.97	0.137	0.963	0.093	0.008
2	9.92	96.91	0.146	0.07	12.69	⋯	2.15	2.01	242.35	11.6	0.033	0.468	0.202	0.012
3	12.81	87.29	0.214	0.025	12.49	⋯	1.62	1.56	125.3	7.91	0.019	0.784	0.042	0.0009
4	−1.41	280.01	0.057	0.134	17.02	+	2.82	2.4	203.26	25.62	0.08	0.597	0.234	0.02
5	4.68	143.72	0.482	0.088	30.99	⋯	2.56	2.05	78.9	60.46	0.112	1.28	0.11	0.031
6	−49.29	298.23	0.272	0.099	16.95	⋯	2.4	2.04	129.44	29.61	0.082	0.829	0.054	0.008
7	−30.97	65.68	0.269	0.211	16.13	+	3.06	2.38	143.06	55.1	0.125	0.595	0.189	0.026
8	−26.53	123.42	0.161	0.131	32.08	+	2.31	1.78	45.3	118.64	0.13	0.989	0.169	0.019
9	0.13	261.51	0.071	0.059	10.77	⋯	2.06	1.9	106.16	22.51	0.042	0.7	0.109	0.015
10	9.77	298.47	0.103	0.066	8.64	⋯	2.41	2.19	182.34	16.09	0.047	0.715	0.221	0.026
11	−64.89	257.61	0.081	0.094	16.8	⋯	2.47	2.23	203.59	18.17	0.051	0.546	0.112	0.018
12	−31.85	268.5	0.119	0.142	10.01	+	2.49	2.29	343.78	16.34	0.043	0.303	0.19	0.03
13	−17.47	83.15	0.173	0.159	28.27	⋯	2.8	2.28	148.26	39.55	0.103	0.648	0.084	0.0033
14	−44.79	75.19	0.248	0.215	26.2	⋯	3.25	2.18	97.11	72.68	0.198	0.921	0.13	0.02
15	−29.08	284.44	0.018	0.201	17.78	⋯	2.76	2.17	153.14	49.06	0.121	0.601	0.101	0.032
16	−65.16	266.74	0.077	0.212	16.4	+	2.55	1.82	113.89	64.04	0.168	0.795	0.136	0.042
17	−81.8	17.46	0.344	0.32	28.36	⋯	3.41	2.4	118.63	87.85	0.173	0.541	0.469	0.159
18	−47.19	288.11	0.041	0.145	39.25	+	2.7	2.06	63.75	83.6	0.135	0.928	0.176	0.093
19	−12.2	245.9	0.105	0.108	19.55	+	2.76	2.41	153.56	29.43	0.067	0.626	0.09	0.046
20	−6.33	81.22	0.297	0.172	16.66	+	2.68	2.4	298.35	21.83	0.054	0.316	0.322	0.053
21	28.65	266.53	0.056	0.055	19.92	⋯	2.91	2.4	55.19	37.67	0.095	1.73	0.348	0.052
22	24.99	80.16	0.038	0.123	7.74	+	2.38	2.18	376.58	13.09	0.046	0.371	0.209	0.044
23	−17.06	90.89	0.14	0.07	40.01	+	2.09	1.65	49.06	51.72	0.117	1.67	0.26	0.102
24	−39.15	258.87	0.143	0.188	9.95	+	3.03	2.39	179.48	38.49	0.118	0.626	1.086	0.195
25	8.49	92.56	0.411	0.291	21.4	+	3.37	2.41	119.96	76.63	0.167	0.573	0.604	0.082

the αR of the Exp-Lundquist model (front boundary); and (f) the αR of the Lundquist model versus the $\alpha R/\tau$ of the Exp-Lundquist model (rear boundary). In these plots, we use three colors to indicate the three types of MEs, as discussed above: red indicates type 1 MEs (13 events), blue indicates type 2 MEs (two events), and green indicates the type 3 MEs (1o events). The output parameters, especially the orientations (θ, ϕ) and radius (R), are very consistent across the two models. The slopes of these distributions are all close to unity. For the distribution of B_0 on the axis (Figure 5 (c)), the values of the Exp-Lundquist model depend on the τ value at the center of the flux rope structures. The ratio of $B_{0\rm ExpL}$ to B_{0L} is about 1.3. Since the output parameters are consistent when using these two models, the results are reliable, and can be used for further discussions (see Al-Haddad et al. 2013). For most parameters, there is no obvious organization of the events by Type, meaning, for example, that Type 1 MEs do not have a lower magnetic field strength than Type 2 or Type 3 MEs.

One exception is the value of αR. Comparing the αR (or $\alpha R/\tau$) at the boundaries, the Exp-Lundquist model's front boundary (αR value) is consistent with the Lundquist model's result (Figure 5(e); the slope is around 1). The Exp-Lundquist model's rear boundary ($\alpha R/\tau$) is about 0.91 times the Lundquist model's boundary value (Figure 5(f); in the fitting equation, the boundary values of 2.4 are not included).

4.3. Comparison of the Goodness of the Fits and Association with the ME Magnetic Field Asymmetry

Figure 6 shows the distributions of the normalized χ^2 values of the B components and $B_{\rm total}$. The panels show, from top left to bottom right: (a) the normalized χ^2 of the B components; (b) the normalized $\chi^2_{B_{total}}$; (c) DiP versus the normalized χ^2 of the B components; (d) DiP versus the normalized $\chi^2_{B_{total}}$; (e) $B_{\rm ratio}$ versus normalized $\chi^2_{B_{total}}$; and (f) S/A versus normalized $\chi^2_{B_{total}}$.

The fits on the three magnetic field components are all quite good when using either of the two models. As shown in Figure 6(a), the normalized χ^2 values of the B components are close for both models, with a few exceptions. Most points have a value of χ^2 between 0.05 and 0.25, with six Type 3 events as

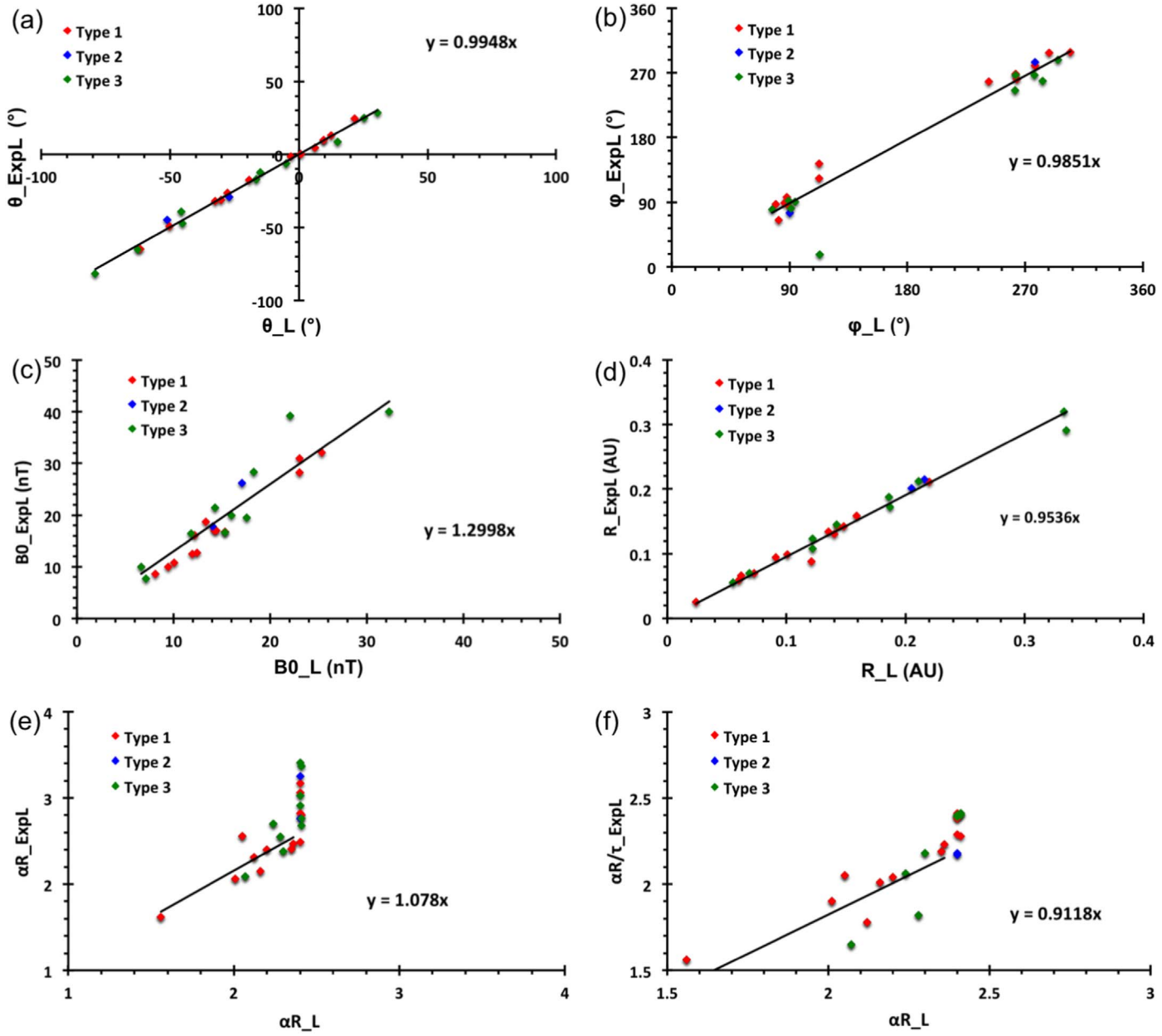

Figure 5. Scatter distributions of the output parameters of the two models: (a) latitude angle, θ (°); (b) longitude angle, ϕ (°); (c) B_0 (nT) on the axis; (d) fitted radius (au); (e) αR of the Lundquist model vs. αR of the Exp-Lundquist model (front boundary); and (f) αR of the Lundquist model vs. $\alpha R/\tau$ of the Exp-Lundquist model (rear boundary). Red indicates Type 1 MEs (13 events), blue indicates Type 2 MEs (two events), and green indicates Type 3 MEs (10 events). For each plot, the best-fit linear relation between the parameter is provided.

the only exceptions. On average, the Exp-Lundquist model has a χ^2 about 4% lower than that of the Lundquist model. There are 18 events that show improvements when using the Exp-Lundquist model, five events with worse fits, and one event that remains unchanged. Type 1 and Type 2 events all have values smaller than 0.25. Some of the normalized χ^2 values of the B components of the Type 3 events are larger than 0.3, but there are also some events here with χ^2 values below 0.2.

Figure 6(b) shows the distribution of the normalized $\chi^2_{B_{total}}$.

The large majority of the studied MEs (21 of 25) have smaller values of $\chi^2_{B_{total}}$ for the Exp-Lundquist model, with an average decrease of 25%, as compared to the Lundquist model. This indicates an improvement from the Exp-Lundquist solution on the fitted $B_{\rm total}$. As discussed in Section 3.2, we classify the MEs into three categories, based on their $\chi^2_{B_{total}}$ value being above or below a threshold of 0.035. Type 1 events have $\chi^2_{B_{total}}$ below this threshold for both models, Type 2 events have it for only the expanding Lundquist model, and Type 3 events have it for none. We emphasize that there are no significant differences in how much the expanding Lundquist model reduces the value of $\chi^2_{B_{total}}$ for different types of MEs.

Figures 6(c) and (d) show the relationships between the DiP and the χ^2 of the magnetic field components and $B_{\rm total}$. DiP indicates the effect of the cross-sectional distortion of $B_{\rm total}$. The DiP values are in the range [0.3, 0.55], with an average of 0.45 and only one event having a DiP greater than 0.51. This indicates that the majority of the events have an asymmetry of the magnetic field toward the front. This figure shows a clear

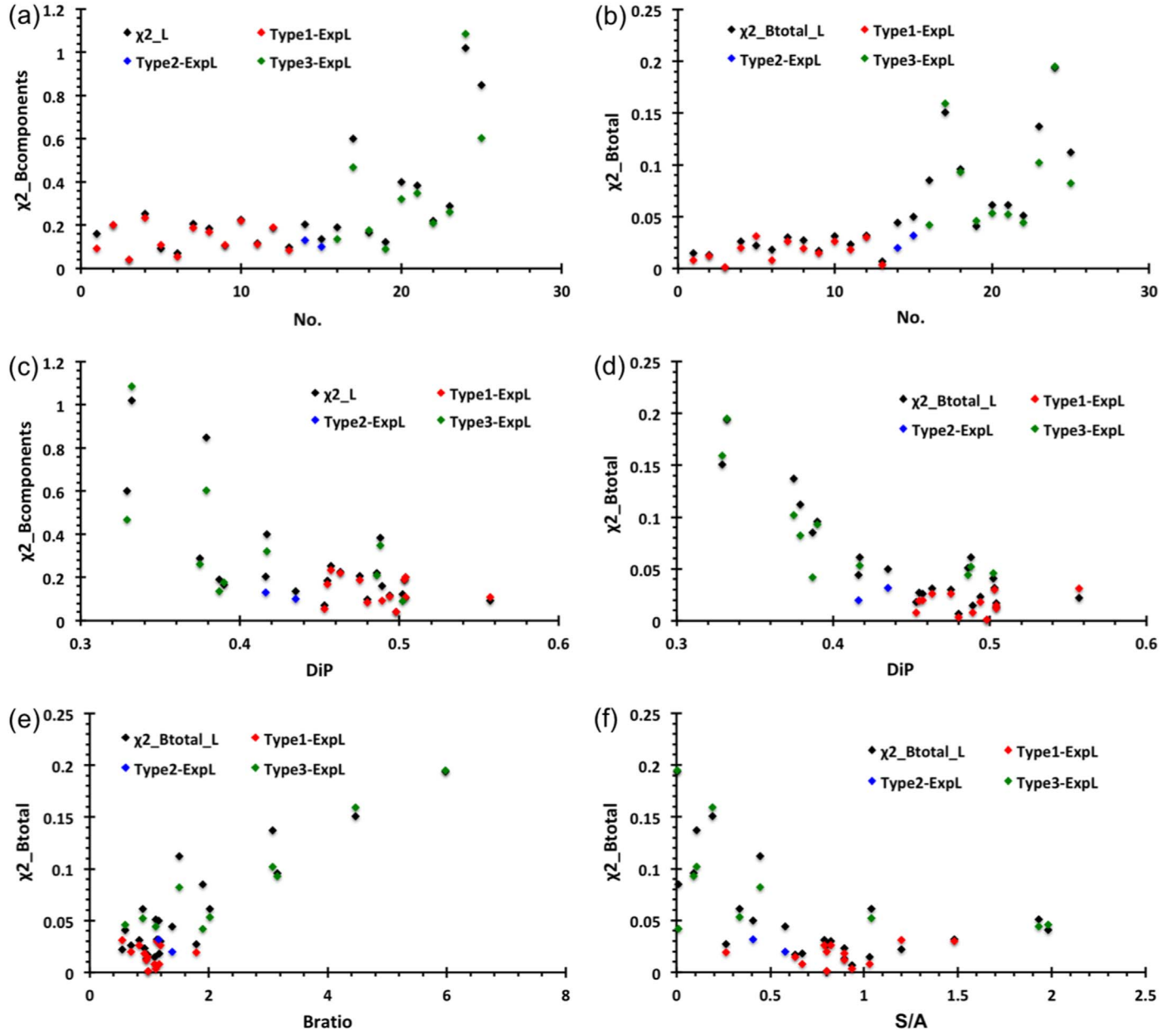

Figure 6. The scatter distributions of the χ^2 values of the two models: (a) normalized χ^2 of the B components; (b) normalized $\chi^2_{B_{total}}$; (c) DiP vs. normalized χ^2 of the B components; (d) DiP vs. normalized $\chi^2_{B_{total}}$; (e) $B_{\rm ratio}$ vs. normalized $\chi^2_{B_{total}}$; and (f) S/A vs. normalized $\chi^2_{B_{total}}$.

relationship between χ^2 (for both the components and $B_{\rm total}$) and DiP, with χ^2 increasing as the DiP values move away from 0.5. For $\chi^2_{B_{total}}$, the anticorrelation between it and the DiP is very clear, especially for those events with DiP < 0.5. We note that at DiP $= 0.45$, the χ^2 value reaches a minimum, and this is especially noticeable for the expanding Lundquist model, with higher values between 0.45 and 0.5. Type 1 (0.487) and Type 3 (0.409) events have statistically different average values of DiP, with the Type 2 events having an intermediate average (0.426). There are no Type 1 events with a DiP below 0.45, meaning that events with even moderate asymmetry in their magnetic field profiles are not well fitted by the nonexpanding Lundquist model. There are only three events with a DiP between 0.4 and 0.45 in our sample, two being Type 2 events and one being Type 3. This seems to indicate that events with moderate asymmetry may be well reproduced with a self-similar expanding model. All events with a DiP lower than 0.40 are Type 3 events, i.e., their asymmetry cannot be explained by a model without expansion nor by a model with self-similar expansion.

Similar results are obtained when looking at the other measure of asymmetry (Figure 6(e), the relationships between $B_{\rm ratio}$ and $\chi^2_{B_{total}}$). $B_{\rm ratio}$ is the ratio of the magnetic field strength at the front boundary to that at the rear boundary. Type 1 events have an average $B_{\rm ratio}$ of 1.03, Type 2 events of 1.28, and Type 3 events of 2.47. This shows that events that are well fitted by the static Lundquist model have a very small front-to-back asymmetry; that those that are well fitted by a self-similar expanding model, based on the velocity measurements, have an asymmetry of ∼25%; and that those that are not well fitted by either model have a larger asymmetry, often reaching over 100%.

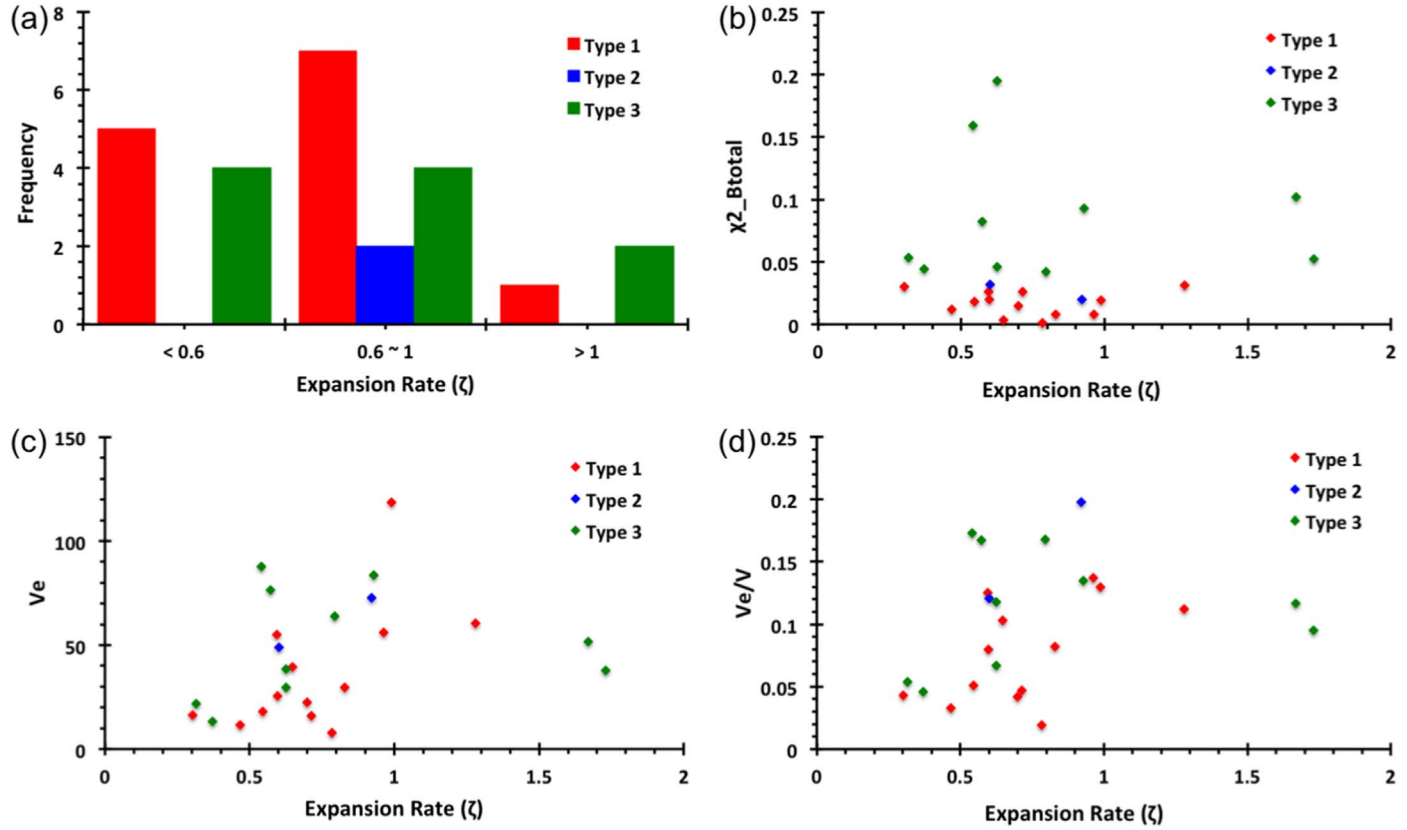

Figure 7. The expansion rate (ζ) of the Exp-Lundquist model and its relationships to the expansion speed and the goodness of fit.

The asymmetry properties of $B_{\rm total}$ are also represented by S/A. S/A represents the position of the peak of $B_{\rm total}$. In Figure 6(f), we present the relationships between S/A versus $\chi^2_{B_{total}}$. The $\chi^2_{B_{total}}$ values are inversely correlated with S/A. An S/A value of [0, 1] indicates that the peak is toward the front (76%), and a value of [1, 2] indicates that it is toward the rear (24%). The position of the peak of the maximum magnetic field has significantly more scatter; however, for Type 1, it is on average within 25% of the center (where $S/A = 1$), for Type 2 it is within 40%, and it can be anywhere for Type 3 events.

4.4. Dimensionless Expansion Rate

We next address the expansion rate (ζ; Figure 7). The distribution of the expansion rate (ζ) is plotted in Figure 7(a). The average ζ of these 25 MEs is around 0.76, which is close to the ζ found by Démoulin et al. (2008) for 26 MCs observed at 1 au (Démoulin & Dasso 2009), and consistent with theoretical expectations for unperturbed events, confirming our criteria for "simple" CMEs. Half of the MEs have a value of ζ in the range of [0.6, 1.0] (52%).

As shown in panels (a) and (b) of Figure 7, there is no clear relationship between the ME type (how well the magnetic field is fitted) and the ζ parameter. The majority of the events (77% of the Type 1 events, all Type 2 events, and 60% of the Type 3 events) have a value of ζ between [0.5, 1]. There is no clear relationship between ζ and V_e, although it has a large range between [10, 120] km s^{-1} (Figure 7(c)), confirming the results of Gulisano et al. (2010) that the use of ζ accounts for the influence of the CME size and speed on the expansion (large and fast CMEs have higher expansion speeds, but are not necessarily expanding more strongly).

There is, however, a statistical difference in terms of $V_e/\langle V\rangle$ at the 95% level (using a standard t-test), even though there is an overlap between the two types (see Figure 7(d)). Type 1 events have an average value of 0.077 versus 0.114 for Type 3 events. Interestingly, the Type 2 events include the event with the largest ratio (0.16). Wang et al. (2005) found that, on average, the expansion speed is about 12% of the CME speed, although Richardson & Cane (2010) only found a weak correlation between these two quantities. Based on that value, however, we can see that the Type 1 events have relatively low expansion, as compared to their speed, and that Type 3 events have typical expansion. Type 3 events may have a higher expansion rate.

4.5. Self-similar Expansion Time

The results for t_0 and its relationship with the goodness of fit and expansion parameters are presented in Figure 8: panel (a) shows t_0 (h) versus $\chi^2_{B_{total}}$; panel (b) shows t_0/T versus the dimensionless expansion rate (ζ; where T is a simple estimate of the ME propagation time from the Sun to 1 au, $T = 1\,AU/V_{sw}$); panel (c) shows t_0 (h) versus V_e/V; and panel (d) shows t_0 (h) versus ζ.

t_0 was obtained by fitting the velocity profile ranges with values from 45 to 380 hr during the Exp-Lundquist fitting process. The t_0 distributions of the three types of MEs are scattered, with no clear relationship between t_0 and the ME type.

There is a clear inverse relationship between t_0 and ζ (as shown in panel (d)). Most of the ζ values fall between [0.5, 1], where the MEs undergo close to self-similar expansion. Within this range, the t_0 values vary from 45 to 200 hr. For t_0/T versus

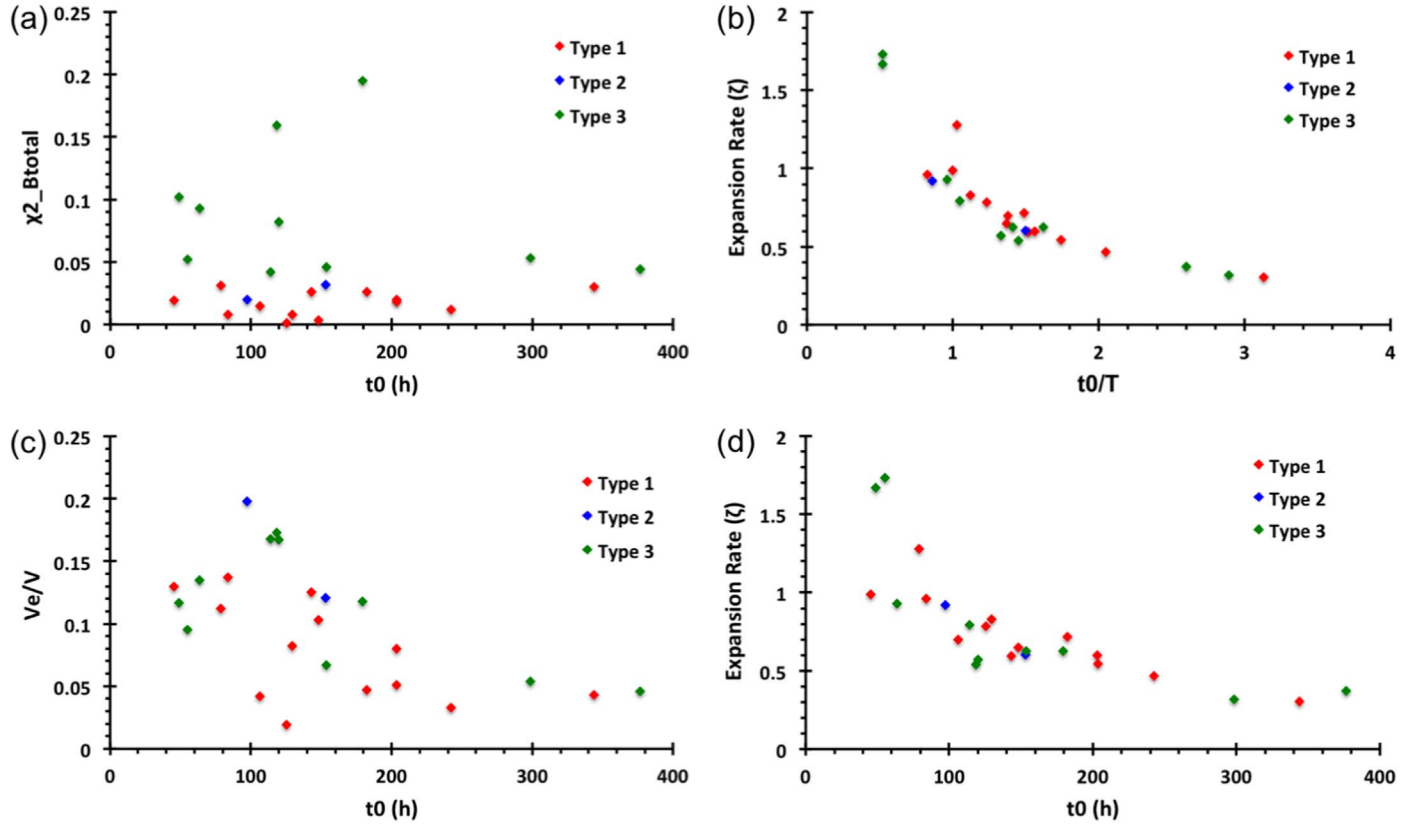

Figure 8. The t_0 of the Exp-Lundquist model.

ζ (Figure 8(b)), the inverse relationship is even clearer. 80% of the MEs have $t_0/T > 1$, which corresponds to $\zeta < 1$. Therefore, the self-similar expansion time t_0 acquired from fitting the velocity profile is larger than the estimated age of the MEs. T is estimated using the final speed (as measured at 1 au) of the ME; it is therefore an upper bound to the CME "age," with the deceleration of the MEs as they propagate resulting in a lower true "age." Therefore, t_0 from the velocity is an even larger proportion of the true CME age as is plotted in Figure 8(b). We therefore conclude that, during the propagation of the MEs, the expansion is not always self-similar. In most of the cases, the expansion rate is stronger than that of self-similar expansion.

5. Summary and Conclusions

In this work, we have selected "simple" MEs from the published CME lists measured in situ by STEREO (Jian et al. 2018) and by the Wind spacecraft. We require these MEs to satisfy the following criteria: (i) they have clear MC-like features (increased $B_{\rm total}$, smooth rotations on the B components, and low T_p or β_p); (ii) the eigenvalue ratio from the MVA is larger than 5 (which indicates a well-defined structure); (iii) the axis obtained from the fitting of the Lundquist force-free solution makes a relatively large angle with respect to the radial direction—the longitude angle ϕ should be between [60°, 120°] or [240°, 300°]; (iv) the dimensionless impact parameter ($|p|$/R) is less than 0.3, as obtained from fitting with the Lundquist model; and (v) the bulk speed is clearly decreasing (as seen in the gradient of the velocity). We arrived at 25 MEs (four from STEREO and 21 from Wind).

The magnetic field components of these 25 MEs can be well fitted by the Lundquist model. However, $B_{\rm total}$ is not reconstructed well in many of the cases, as the total magnetic field has a peak in the front half of the ME in almost all cases. As these MEs have clear radial expansion (as seen from the decreasing bulk speed profile), we test whether or not the expansion is the main reason for the shift of the total magnetic field magnitude. To do so, we introduce the Exp-Lundquist model, which considers the expansion when deriving the solutions of the B components (Farrugia et al. 1992).

We compare the fitting results of these two models in order to find out whether the Exp-Lundquist model is better at reconstructing the magnetic field structures of these simple MEs (especially the shift of $B_{\rm total}$). By eye, both models fit the three magnetic field components very well (given the close χ^2 numbers of the B components), and the Exp-Lundquist model returns smaller values of $\chi^2_{B_{total}}$. We define a threshold for $\chi^2_{B_{total}}$ of 0.035 and classify the 25 MEs into three types: (i) MEs that are well fitted by both models (13 events), as both the static and expanding fitting models return a χ^2 below the threshold; (ii) MEs that are well fitted by the Exp-Lundquist model, but not by the static Lundquist model (two events); and (iii) MEs that are not adequately fitted by either model (10 events).

In general, the results (orientation, ME size, and magnetic field strength) are consistent for these simple MEs between the static and expanding versions of the force-free fitting models. We then compare the types of MEs (i.e., the capacity of the static and expanding models to fit the total magnetic field) with different measures of ME asymmetry, including the DiP of Nieves-Chinchilla et al. (2018), the ratio of the magnetic field strength at the front to that at the back boundary, and the position of the peak in the magnetic field within the ME. The

DiP values of these 25 MEs are in the range of [0.3, 0.55], with an average of 0.45 and only one event having a DiP greater than 0.51. The large majority of our events have an asymmetry of the magnetic field toward the front, which is consistent with past studies (Nieves-Chinchilla et al. 2018; Démoulin et al. 2020).

Type 1 events have an average $B_{\rm ratio}$ of 1.03, Type 2 events have a ratio of 1.28, and Type 3 events have a ratio of 2.47. This shows that events that are well fitted by the static Lundquist model have little front-to-back asymmetry, those that are well fitted by an expanding model have an asymmetry of ∼25%, and those that are not well fitted by either model have larger asymmetry, often reaching over 100%.

Overall, we find that MEs with very small asymmetry of the magnetic field profile can be well fitted by a static force-free model, whereas events with moderate asymmetry (DiP ∼0.4–0.45, for example) can be well fitted by a force-free model with self-similar expansion, with the expansion being determined by the profile of the plasma velocity. However, for events with larger asymmetry, the expansion alone cannot explain the entire asymmetry, a result that is consistent with recent work using different methods (Démoulin et al. 2020).

Our results indicate that the shift of the magnetic field peak toward the front is only partially due to expansion. Between this and the findings of Démoulin et al. (2020), that the asymmetry of $B_{\rm total}$ is not solely caused by aging, other physical factors are necessary to explain the asymmetry of $B_{\rm total}$.

We have also investigated whether or not the expansion is self-similar. The average dimensionless expansion parameter, ζ, of these 25 MEs is 0.76, which is close to the average value of ζ found by Démoulin et al. (2008) for 26 unperturbed MCs observed at 1 au. There is no statistical difference between the dimensionless expansion parameter as measured by ζ between different types of MEs. However, Type 2 MEs tend to have high ratios of the expansion to propagation speeds, reaching up to 20%, as compared to typical values closer to 10%. This may indicate that only these events with large expansion as compared to their propagation speeds evolve close to self-similarly, or they may be artifacts, due to the small number of events considered.

We have also examined the relationship between t_0 (h) and ζ. t_0 is derived from the velocity profile, and corresponds to the self-similar expansion time before the MC encounters the spacecraft. In Farrugia et al. (1993b), the authors hypothesized that t_0 should correspond to the ME age; i.e., they hypothesized that MEs expand self-similarly from the Sun to the Earth. There is a clear inverse relationship between t_0 (h) and ζ, indicating that both are good ways of quantifying the CME expansion. We use $T = 1AU/V_{sw}$ to estimate the upper bound of the age of the ME. We derive t_0/T to compare the self-similar expansion time and the age of ME. We find that more than 80% of MEs have $t_0/T > 1$. That is, the self-similar expanding time t_0 is larger than the age of the ME. This gives a strong indication that the expansion of the MEs during their propagation from the Sun to 1 au is stronger than self-similar expansion.

We conclude that the assumption of self-similar expansion is not correct for most events, as a self-similar expanding force-free field model is not able to fit the observed asymmetry of the magnetic field profile. Our results are consistent with the recent findings of Démoulin et al. (2020). While the expansion time, t_0, obtained from the velocity profile is usually larger than the estimated age, the expansion rate should be larger than self-similar. However, ζ usually lies in the self-similar expanding range. If the ME expansion is faster than self-similar in the innermost heliosphere (below 0.5–0.7 au), as hypothesized by Lugaz et al. (2020b), this could explain why the magnetic field is more asymmetric than that obtained using the assumption of self-similar evolution from the Sun to the Earth. Obtaining more measurements of CME magnetic fields and velocities in the innermost heliosphere will now be possible, and the Parker Solar Probe (Fox et al. 2016) and Solar Orbiter (Müller et al. 2020) shall help to determine whether this is the case. In addition, comparisons between remote observations of CME expansions in the corona and inner heliosphere with in situ measurements of CME expansions should also help. Finally, it is also possible that other factors play a role in the magnetic field asymmetry of MEs. The first possibility is that MEs have a non-force-free structure or a non–flux rope structure (Al-Haddad et al. 2011). The second possibility is that there is additional aging of the MEs, beyond the changes due to expansion (for example, the magnetic field is still evolving and the speed is still changing significantly over the duration of an ME's passage over a spacecraft near 1 au). This could be tested by obtaining more multispacecraft measurements of MEs and by investigating the changes in the additional aging of ME properties over a timescale of one day, the typical duration of an ME near 1 au. Future work should focus on determining whether or not this is indeed the case.

W.Y. and N.A. acknowledge support from NSF AGS-1954983 and NASA ECIP 80NSSC21K0463.

W.Y. and F.R. acknowledge support from NASA 80NSSC20K0431, NASA ECIP 80NSSC21K0463, and NASA STEREO 80NSSC20K0431.

N.L. acknowledges support from NASA HSR 80NSSC19K0831 and HGI 80NSSC20K0700.

A.G. acknowledges support from NASA STEREO 80NSSC20K0431.

C.F. acknowledges support from NASA STEREO 80NSSC20K0431 and NASA 80NSSC19K1293.

ORCID iDs

Wenyuan Yu https://orcid.org/0000-0002-2917-5993
Nada Al-Haddad https://orcid.org/0000-0002-0973-2027
Charles J. Farrugia https://orcid.org/0000-0001-8780-0673
Noé Lugaz https://orcid.org/0000-0002-1890-6156
Florian Regnault https://orcid.org/0000-0002-4017-8415
Antoinette Galvin https://orcid.org/0000-0003-3752-5700

References

Al-Haddad, N., Galvin, A. B., Lugaz, N., Farrugia, C. J., & Yu, W. 2022, ApJ, 927, 68
Al-Haddad, N., Nieves-Chinchilla, T., Möstl, C., et al. 2013, SoPh, 284, 129
Al-Haddad, N., Nieves-Chinchilla, T., Savani, N. P., Lugaz, N., & Roussev, I. I. 2018, SoPh, 293, 73
Al-Haddad, N., Roussev, I. I., Möstl, C., et al. 2011, ApJL, 738, L18
Bothmer, V., & Schwenn, R. 1998, AnGeo, 16, 1
Burlaga, L., Sittler, E., Mariani, F., & Schwenn, R. 1981, JGR, 86, 6673
Burlaga, L. F. 1988, JGR, 93, 7217
Cid, C., Hidalgo, M. A., Nieves-Chinchilla, T., Sequeiros, J., & Viñas, A. F. 2002, SoPh, 207, 187
Davies, E. E., Möstl, C., Owens, M. J., et al. 2021, A&A, 656, A2
Démoulin, P., & Dasso, S. 2009, A&A, 507, 969
Démoulin, P., Dasso, S., Lanabere, V., & Janvier, M. 2020, A&A, 639, A6
Démoulin, P., Nakwacki, M. S., Dasso, S., & Mandrini, C. H. 2008, SoPh, 250, 347

Farrugia, C. J., Burlaga, L. F., Osherovich, V. A., et al. 1993a, JGR, 98, 7621
Farrugia, C. J., Burlaga, L. F., Osherovich, V. A., & Lepping, R. P. 1992, in Solar Wind Seven Colloquium, ed. E. Marsch & R. Schwenn (Goslar: COSPAR), 611
Farrugia, C. J., Freeman, M. P., Burlaga, L. F., Lepping, R. P., & Takahashi, K. 1993b, JGR, 98, 7657
Farrugia, C. J., Janoo, L. A., Torbert, R. B., et al. 1999, AIP Conf. Proc., 471, 745
Fox, N. J., Velli, M. C., Bale, S. D., et al. 2016, SSRv, 204, 7
Gold, T., & Hoyle, F. 1960, MNRAS, 120, 89
Gulisano, A. M., Démoulin, P., Dasso, S., Ruiz, M. E., & Marsch, E. 2010, A&A, 509, A39
Hidalgo, M. A. 2003, JGR, 108, 1320
Hidalgo, M. A. 2005, JGR, 110, A03207
Hidalgo, M. A., Nieves-Chinchilla, T., & Cid, C. 2002, GeoRL, 29, 130000
Hu, Q., Qiu, J., & Krucker, S. 2015, JGR, 120, 5266
Jian, L. K., Russell, C. T., Luhmann, J. G., & Galvin, A. B. 2018, ApJ, 855, 114
Klein, L. W., & Burlaga, L. F. 1982, JGR, 87, 613
Lepping, R. P., Berdichevsky, D. B., & Wu, C.-C. 2017, SoPh, 292, 27
Lepping, R. P., Burlaga, L. F., & Jones, J. A. 1990, JGR, 95, 11957
Lopez, R. E. 1987, JGR, 92, 11189
Lugaz, N., Farrugia, C. J., Winslow, R. M., et al. 2017, ApJ, 848, 75
Lugaz, N., Salman, T. M., Winslow, R. M., et al. 2020a, ApJ, 899, 119
Lugaz, N., Winslow, R. M., & Farrugia, C. J. 2020b, JGRA, 125, e27213
Lundquist, S. 1950, Ark. Fys., 2, 361
Moldwin, M. B., Ford, S., Lepping, R., Slavin, J., & Szabo, A. 2000, GeoRL, 27, 57
Moldwin, M. B., Phillips, J. L., Gosling, J. T., et al. 1995, JGR, 100, 19903
Müller, D., Cyr, O. C., Zouganelis, I., et al. 2020, A&A, 642, A1
Nieves-Chinchilla, T., Vourlidas, A., Raymond, J. C., et al. 2018, SoPh, 293, 25
Osherovich, V. A., Farrugia, C. J., & Burlaga, L. F. 1993, AdSpR, 13, 57
Richardson, I. G., & Cane, H. V. 2010, SoPh, 264, 189
Salman, T. M., Lugaz, N., Farrugia, C. J., et al. 2020, ApJ, 904, 177
Vandas, M., Romashets, E. P., Watari, S., et al. 2006, AdSpR, 38, 441
Wang, C., Du, D., & Richardson, J. D. 2005, JGR, 110, A10107
Wang, Y., Zhou, Z., Shen, C., Liu, R., & Wang, S. 2015, JGR, 120, 1543
Yu, W., Farrugia, C. J., Lugaz, N., et al. 2014, JGR, 119, 689
Yu, W., Farrugia, C. J., Lugaz, N., et al. 2018, SoPh, 293, 165